Research in Astron. Astrophys. **2010** Vol. **10** No. **1**, 67 – 82
http://www.raa-journal.org *http://www.iop.org/journals/raa*

Research in Astronomy and Astrophysics

A search for massive young stellar objects with 98 CH_3OH maser sources *

Tie Liu, Yue-Fang Wu and Ke Wang

Department of Astronomy, Peking University, Beijing 100871, China; *yfwu@vega.bac.pku.edu.cn*

Received 2008 July 10; accepted 2009 October 23

Abstract Using the 13.7 m telescope of the Purple Mountain Observatory (PMO), a survey of the $J = 1 - 0$ lines of CO and its isotopes was carried out on 98 methanol maser sources in January 2008. Eighty-five sources have infrared counterparts within one arcmin. In the survey, except for 43 sources showing complex or multiple-peak profiles, almost all the ^{13}CO line profiles of the other 55 sources have large line widths of 4.5 km s^{-1} on average and are usually asymmetric. Fifty corresponding Infrared Astronomical Satellite (IRAS) sources of these 55 sources have $L_{\rm bol}$ larger than $10^3\,L_\odot$, which can be identified as possible high-mass young stellar sources. Statistics show that the ^{13}CO line widths correlate with the bolometric luminosity of the associated IRAS sources. Here, we also report the mapping results of two sources: IRAS 06117+1350 and IRAS 07299–1651. Two cores were found in IRAS 06117+1350 and one core was detected in IRAS 07299–1651. The northwest core in IRAS 06117+1350 and the core in IRAS 07299–1651 can be identified as precursors of UC HII regions or high-mass protostellar objects (HMPOs). The southeast core of IRAS 06117+1350 has no infrared counterpart, seeming to be at a younger stage than the pre-UC HII phase.

Key words: stars: formation — ISM: clouds — ISM: methanol maser

1 INTRODUCTION

The formation and evolution of massive stars is still a mystery and our understanding of how high-mass stars form and evolve lags behind that of low-mass stars, which is understood better using the theory constructed by Shu et al. (1987). High-mass stars can produce an enormous impact on their local environment and the evolution of the whole Galaxy. However, due to their distant location, growth and development in clusters and short evolutionary time scales, it is difficult to find samples of high-mass young sources to investigate their formation processes.

In the past, interstellar H_2O masers (e.g. Plume et al. 1992; Wu et al. 2006) were used as tracers for high-mass star formation regions in the early evolutionary phase. However, H_2O masers can also be found in low-mass star formation regions (e.g.,Wu et al. 2004), while methanol (CH_3OH) masers seem to be exclusively associated with high-mass star formation regions (e.g. Minier et al. 2003). Methanol masers are traditionally divided into two classes. Class II methanol masers are found in the vicinity of high-mass young stellar objects, while Class I methanol masers are believed to trace

∗ Supported by the National Natural Science Foundation of China.

distant parts of the outflows from these high-mass star formation regions (Sobolev et al. 2005). With the motivation of finding more pre-UC HII regions or even more earlier high-mass stellar objects, we carried out a survey of $J = 1 - 0$ lines of ^{12}CO and its isotopes ^{13}CO and C^{18}O on 98 methanol maser sources. The next section describes the observations. The survey results and mapping results will be given and discussed in Section 3. Section 4 summarizes the paper.

2 OBSERVATIONS

The observations were made in January 2008 with the 13.7 m telescope of PMO at Qinghai Station. The ^{12}CO, ^{13}CO and C^{18}O ($J = 1 - 0$) lines were observed simultaneously by a superconductor receiver. The back-end is equipped with three acousto-optic spectrometers (AOSs). Every spectrometer has 1024 channels. The total bandwidths were 145.330 MHz, 42.762 MHz and 43.097 MHz for ^{12}CO, ^{13}CO and C^{18}O lines, corresponding to velocity resolutions of 0.37, 0.11 and 0.12 km s^{-1}, respectively. The system temperatures during the observation ranged from 200 K to 350 K (SBD), depending on the weather. The half-power beamwidth (HPBW) at 112 GHz was $\sim 59''$. The pointing accuracy of the telescope was better than $8''$, and the main beam efficiency at the zenith was about 0.67.

We adopted the position switch mode for all the spectral measurements. Our mapping steps toward right ascension and declination directions were both 1 arcmin. The integrating time was ∼3 minutes per position. The noise level of the antenna temperature $T_A{}^*$ was usually about 0.4 K for the ^{12}CO, 0.3 K for the ^{13}CO and 0.2 K for the C^{18}O ($J = 1 - 0$) band. For the data analysis, the GILDAS software package including CLASS and GREG was employed (Guilloteau & Lucas 2000).

3 RESULTS AND DISCUSSION

3.1 Sample Analysis

Ninety-eight sources were observed, 29 of which belong to Class I methanol masers. Table 1 presents basic parameters of all the sources surveyed. The associated IRAS sources within $3' \times 3'$ are presented in Col. (2). Eighty-five have IR counterpart candidates within one arcmin. Cols. (3)–(6) give the equatorial coordinates and the Galactic coordinates, respectively. The color indices log(F_{25}/F_{12}) and log(F_{60}/F_{12}) are presented in Cols. (7)–(8) (F_{12}, F_{25}, and F_{60} represent the flux at 12 μm, 25 μm and 60 μm, respectively). Col. (9) lists the fluxes at 100 μm. The types of these methanol masers and the related references are placed in Cols. (10)–(11).

Figure 1 shows the distribution of the sources surveyed in Galactic coordinates. The sample sources are concentrated on the Galactic plane ($|b| < 2°$) and about 90% are found in the first quadrant. Only Orion's source has $|b| > 15°$, and 72 sources are located in $0 < l < 45°$.

The locations of the associated IRAS sources in the color-color planes are plotted in Figure 2. The distributions show that about 75% of the Class I and 63% of the Class II methanol maser sources observed have IRAS color indices satisfying the criteria of the UC HII regions established by Wood & Churchwell (1989). All of these UC HII region candidates, except for Orion's source, have fluxes larger than 100 Jy at 100 μm.

3.2 Survey Results and Discussion

All the 98 sources are detected with $J = 1 - 0$ lines of ^{12}CO, ^{13}CO and C^{18}O. Forty-three sources have too-complex line profiles and will be studied further. The other fifty-five sources were analyzed, including 17 Class I methanol maser sources. Figure 3 presents the spectra of all the 55 sources and one source, IRAS 18403–0417, which has blended lines. The gray, green and red lines represent ^{12}CO, ^{13}CO and C^{18}O respectively. The ^{12}CO spectra of IRAS 18414–1723, IRAS 18353–0628,

Table 1 Parameters of All the Sources Surveyed

Name	IRAS No.	α(B1950) (h m s)	δ(B1950) (° ′ ″)	l °	b °	$\log\left(\frac{F_{25}}{F_{12}}\right)$	$\log\left(\frac{F_{60}}{F_{12}}\right)$	Flux100 (Jy)	Type	Reference
(1)	(2)	(3)	(4)	(5)	(6)	(7)	(8)	(9)	(10)	(11)
02455+6034	02455+6034	02 45 30.1	+60 34 34.5	136.84	1.14	0.67	1.51	3.395×10^2	II	Szymczak et al. (2000)
05274+3345	05274+3345	05 27 27.59	+33 45 37.32	174.20	–0.08	1.00	1.81	9.057×10^2	II	Szymczak et al. (2000)
Orion’s	05327–0529	05 32 44.8	–05 26 00.0	209.01	–19.41	1.03	2.15	2.448×10^1	I	Haschick et al. (1989)
06056+2131	06056+2131	06 05 40.9	+21 31 32.4	189.03	0.79	0.70	1.55	2.563×10^3	II	Szymczak et al. (2000)
G188.9+0.9	06058+2138	06 05 54.0	+21 39 09.4	188.95	0.89	1.00	1.83	1.666×10^3	I	Haschick et al. (1989)
06099+1800	06099+1800	06 09 57.90	+18 00 11.95	192.60	–0.05	0.54	1.47	5.285×10^3	II	Szymczak et al. (2000)
06117+1350	06117+1350	06 11 46.4	+13 50 32.7	196.45	–1.68	0.90	1.89	1.965×10^3	II	Szymczak et al. (2000)
07299–1651	07299–1651	07 29 55.0	–16 51 47.2	232.62	1.00	1.67	2.37	1.269×10^3	II	Szymczak et al. (2000)
G8.68–0.37	18032–2137	18 03 21.69	–21 37 42.27	8.68	–0.36	0.91	2.00	5.221×10^3	II	Caswell et al. (1993)
G10.47+0.03	18056–1952	18 05 40.54	–19 52 25.30	10.47	0.03	1.13	2.67	1.016×10^4	II	Caswell et al. (1993)
G10.30–0.15	18060–2005	18 05 57.93	–20 06 25.58	10.30	–0.15	0.87	1.63	1.201×10^4	I	Bachiller et al. (1990)
18067–1927	18067–1927	18 06 44.00	–19 27 02.90	10.96	0.02	0.87	2.10	1.292×10^3	II	Szymczak et al. (2000)
G10.6–0.4	18075–1956	18 07 30.6	–19 56 28.3	10.62	–0.38	0.80	2.61	2.137×10^4	I	Haschick et al. (1989)
G12.89+0.49	18089–1732	18 08 56.49	–17 32 14.46	12.89	0.49	0.87	2.31	3.148×10^3	I	Slysh et al. (1994)
G12.03–0.04	18090–1832	18 09 05.59	–18 32 44.17	12.02	–0.03	0.71	1.63	1.710×10^3	II	Caswell et al. (1993)
18092–1842	18092–1842	18 09 13.78	–18 42 19.77	11.90	–0.14	0.10	1.46	1.710×10^3	II	Szymczak et al. (2000)
G11.90–0.14	18092–1842	18 09 14.78	–18 42 20.84	11.90	–0.14	0.10	1.46	1.710×10^3	II	Caswell et al. (1993)
18108–1759	18108–1759	18 10 52.41	–17 59 35.92	12.71	–0.13	0.38	1.88	2.878×10^3	II	Szymczak et al. (2000)
G12.68–0.18	18112–1801	18 11 00.55	–18 02 47.51	12.68	–0.19	0.64	1.77	6.502×10^3	II	Caswell et al. (1993)
G11.94–0.62	18110–1854	18 11 04.4	–18 54 19.8	11.94	–0.62	1.21	2.19	4.930×10^3	I	Bachiller et al. (1990)
W33-Met	18108–1759	18 11 15.78	–17 56 52.62	12.80	–0.19	0.38	1.88	2.878×10^3	I	Haschick et al. (1990)
W33A	18117–1753	18 11 44.56	–17 52 55.71	12.91	–0.26	1.11	2.02	6.310×10^3	I	Haschick et al. (1989)
G12.91–0.26	18117–1753	18 11 45.36	–17 53 09.77	12.91	–0.27	1.11	2.02	6.310×10^3	II	Caswell et al. (1993)
18128–1640	18128–1640	18 12 51.82	–16 40 00.54	14.10	0.09	0.38	1.48	1.017×10^3	II	Szymczak et al. (2000)
18144–1723	18144–1723	18 14 29.81	–17 23 22.70	13.66	–0.60	0.56	1.61	1.137×10^3	II	Szymczak et al. (2000)
G14.33–0.64	18160–1647	18 16 00.9	–16 49 06.3	14.33	–0.65	0.94	2.24	2.819×10^3	I	Slysh et al. (1994)
M17(3)	18174–1612	18 17 31.03	–16 12 49.82	15.04	–0.67	0.89	1.71	6.589×10^4	I	Bachiller et al. (1990)
G15.03–0.68	18174–1612	18 17 31.72	–16 13 06.87	15.03	–0.68	0.89	1.71	6.589×10^4	II	Caswell et al. (1993)
18181–1534	18181–1534	18 18 06.73	–15 34 36.38	15.66	–0.50	–0.26	1.34	6.839×10^2	II	Szymczak et al. (2000)
G16.59–0.06	18182–1433	18 18 20.41	–14 33 18.33	16.59	–0.06	1.15	2.23	1.071×10^3	I	Slysh et al. (1994)
18220–1241	18220–1241	18 22 02.53	–12 41 00.36	18.66	0.03	1.06	2.23	1.095×10^3	II	Szymczak et al. (2000)
G20.24+0.07	18249–1116	18 24 57.15	–11 16 48.95	20.24	0.07	0.24	1.53	3.696×10^2	II	Caswell et al. (1993)
18249–1116	18249–1116	18 24 57.16	–11 16 41.95	20.24	0.07	0.24	1.53	3.696×10^2	II	Szymczak et al. (2000)
18278–1009	18278–1009	18 27 49.62	–10 09 19.38	21.56	–0.03	0.51	1.14	2.284×10^2	II	Szymczak et al. (2000)
G22.34–0.16	18297–0931	18 29 47.29	–09 31 25.86	22.34	–0.16	–0.26	0.48	2.823×10^2	II	Szymczak et al. (2002)
G22.43–0.17	18297–0931	18 29 59.07	–09 27 31.70	22.42	–0.17	–0.26	0.48	2.823×10^2	II	Caswell et al. (1993)
18316–0602	18316–0602	18 31 39.0	–06 02 07.8	25.65	1.05	0.78	1.62	2.136×10^3	II	Slysh et al. (1999)
18317–0859	18317–0859	18 31 44.83	–08 59 41.32	23.04	–0.34	0.18	1.77	1.940×10^2	II	Szymczak et al. (2000)
G23.01–0.41	18318–0901	18 31 56.26	–09 03 15.14	23.01	–0.41	0.70	2.50	4.393×10^3	II	Caswell et al. (1993)
G23.01–0.41	18318–0901	18 31 56.76	–09 03 18.18	23.01	–0.42	0.70	2.50	4.393×10^3	I	Slysh et al. (1994)
18322–0721	18322–0721	18 32 13.56	–07 21 42.32	24.54	0.31	–0.13	1.25	2.935×10^2	I	Szymczak et al. (2000)
18326–0751	18326–0751	18 32 38.38	–07 51 13.13	24.15	–0.01	0.79	2.09	5.740×10^2	I	Szymczak et al. (2000)
18335–0713	18335–0713	18 33 30.13	–07 13 09.83	24.81	0.10	0.96	1.98	6.936×10^3	II	Szymczak et al. (2000)
MMI–117	18335–0714	18 33 30.36	–07 14 41.97	24.79	0.08	0.96	1.98	6.936×10^3	I	Val’tts et al. (2007)
18353–0628	18353–0628	18 35 23.8	–06 28 07.0	25.70	0.03	0.81	1.59	2.435×10^3	II	Szymczak et al. (2000)
MMI–119	18379–0546	18 37 58.3	–05 46 28.0	26.61	–0.22	0.91	1.86	5.343×10^2	I	Val’tts et al. (2007)
MMI–121	18391–0504	18 39 11.55	–05 04 24.47	27.37	–0.16	–0.15	0.59	1.633×10^3	I	Val’tts et al. (2007)
G28.85+0.50	18396–0322	18 39 35.13	–03 27 23.91	28.85	0.50	0.37	1.13	4.073×10^2	II	Blaszkiewicz & Kus (2004)
G28.15+0.00	18402–0418	18 40 02.45	–04 18 20.91	28.15	0.00	0.33	2.80	5.877×10^2	II	Szymczak et al. (2002)
G28.53+0.12	18403–0354	18 40 19.50	–03 55 00.11	28.53	0.12	–0.39	1.04	2.437×10^2	II	Szymczak et al. (2002)
18403–0417	18403–0417	18 40 19.58	–04 17 01.13	28.20	–0.05	0.91	1.86	3.937×10^3	II	Szymczak et al. (2000)
18416–0420	18416–0420	18 41 39.81	–04 20 59.88	28.29	–0.38	0.95	1.57	4.358×10^3	II	Szymczak et al. (2000)
G28.83–0.25	18421–0349	18 42 11.63	–03 49 01.14	28.83	–0.25	1.04	2.11	1.877×10^3	II	Caswell et al. (1993)
G29.86–0.05	18434–0242	18 43 24.69	–02 48 40.33	29.86	–0.05	0.89	1.54	1.167×10^4	II	Szymczak et al. (2002)
G29.95–0.02	18434–0242	18 43 27.0	–02 42 45.5	29.95	–0.02	0.89	1.54	1.167×10^4	II	Caswell et al. (1993)
G30.69–0.06	18449–0207	18 44 58.94	–02 04 27.03	30.70	–0.06	0.64	2.26	4.025×10^3	I	Slysh et al. (1994)

Table 1 — *Continued.*

Name	IRAS No.	α(B1950) (h m s)	δ(B1950) (° ′ ″)	l °	b °	$\log\left(\frac{F_{25}}{F_{12}}\right)$	$\log\left(\frac{F_{60}}{F_{12}}\right)$	Flux100 (Jy)	Type	Reference
(1)	(2)	(3)	(4)	(5)	(6)	(7)	(8)	(9)	(10)	(11)
MMI–125	18449–0207	18 44 58.96	–02 04 26.97	30.70	–0.06	0.64	2.26	4.025×10^3	I	Val'tts et al. (2007)
MMI–127	18449–0115	18 44 59.2	–01 16 10.6	31.41	0.31	1.11	2.43	2.815×10^3	I	Val'tts et al. (2007)
G30.8–0.1	18449–0158	18 45 11.06	–01 57 56.89	30.82	–0.06	0.80	1.81	1.908×10^4	I	Haschick et al. (1989)
G31.28+0.06	18456–0129	18 45 36.80	–01 29 51.71	31.28	0.06	1.26	2.34	3.693×10^3	II	Caswell et al. (1993)
18456–0129	18456–0129	18 45 39.70	–01 29 48.92	31.29	0.05	1.26	2.34	3.693×10^3	II	Szymczak et al. (2000)
G32.74–0.07?	18487–0015	18 48 47.51	–00 15 48.25	32.74	–0.08	0.36	1.89	1.071×10^3	II	Caswell et al. (1993)
18497+0022	18497+0022	18 49 46.43	+00 22 05.59	33.41	–0.002	0.37	1.61	2.064×10^3	II	Szymczak et al. (2000)
G33.74–0.15	18509+0035	18 50 53.88	+00 35 14.80	33.74	–0.15	0.19	2.68	1.757×10^2	II	Szymczak et al. (2002)
G33.64–0.21	18509+0027	18 50 55.54	+00 28 11.68	33.64	–0.21	–0.09	0.95	5.536×10^2	II	Blaszkiewicz & Kus (2004)
G35.05–0.52	18546+0139	18 54 37.21	+01 35 01.02	35.05	–0.52	–0.26	0.19	1.487×10^3	I	Bachiller et al. (1990)
G35.79–0.17	18547+0223	18 54 45.12	+02 23 41.49	35.79	–0.17	0.11	1.67	2.739×10^2	II	Szymczak et al. (2002)
G35.19–0.74	18556+0136	18 55 40.43	+01 36 33.55	35.20	–0.74	1.71	2.66	1.124×10^3	II	Caswell et al. (1993)
G37.60+0.42	18559+0416	18 55 59.7	+04 16 26.3	37.60	0.42	0.18	1.36	2.451×10^2	II	Szymczak et al. (2002)
G37.02–0.03	18566+0330	18 56 30.24	+03 33 30.11	37.02	–0.03	–0.24	0.24	1.553×10^2	II	Szymczak et al. (2002)
18577+0358	18577+0358	18 57 45.20	+03 58 19.84	37.53	–0.11	0.86	1.88	1.867×10^3	II	Blaszkiewicz & Kus (2004)
G39.10+0.48	18585+0538	18 58 32.19	+05 38 09.59	39.10	0.48	–0.03	1.57	1.734×10^2	II	Szymczak et al. (2002)
G35.20–1.73	18592+0108	18 59 12.72	+01 09 14.56	35.20	–1.73	0.95	1.95	1.396×10^4	II	Caswell et al. (1993)
W48	18592+0108	18 59 13.82	+01 09 13.49	35.20	–1.74	0.95	1.95	1.396×10^4	I	Haschick et al. (1989)
18592+0108	18592+0108	18 59 14.6	+01 08 46.4	35.20	–1.75	0.95	1.95	1.396×10^4	II	Szymczak et al. (2000)
19031+0621	19031+0621	19 03 09.87	+06 21 31.12	40.27	–0.20	1.26	2.48	3.658×10^2	II	Szymczak et al. (2000)
19078+0901	19078+0901	19 07 51.8	+09 01 10.5	43.17	0.00	1.01	1.86	3.615×10^4	II	Szymczak et al. (2000)
MMI–134	19092+0841	19 09 14.96	+08 41 34.73	43.04	–0.45	0.51	1.82	5.105×10^2	I	Val'tts et al. (2007)
19095+0930	19095+0930	19 09 30.29	+09 30 41.71	43.79	–0.13	1.39	2.51	2.744×10^3	II	Szymczak et al. (2000)
G43.8–0.1	19099–0934	19 09 31.26	–09 30 51.10	26.83	–8.88	0.14	0.26	2.480×10^0	I	Haschick et al. (1989)
MMI-138	19120+1103	19 12 04.6	+11 04 22.5	45.47	0.05	0.91	1.83	7.890×10^3	I	Val'tts et al. (2007)
19186+1440	19186+1440	19 18 39.8	+14 40 58.0	49.41	0.33	0.53	1.76	1.710×10^2	II	Blaszkiewicz & Kus (2004)
19211+1432	19211+1432	19 21 10.45	+14 32 18.69	49.57	–0.27	0.41	1.42	6.230×10^1	II	Szymczak et al. (2000)
MMI–143	19213+1424	19 21 19.66	+14 25 14.97	49.49	–0.36	1.01	-1.95	2.676×10^4	I	Val'tts et al. (2007)
G49.49–0.37	19213+1424	19 21 22.31	+14 25 07.88	49.49	–0.37	1.01	-1.95	2.676×10^4	II	Caswell et al. (1993)
19216+1429	19216+1429	19 21 37.3	+14 29 51.9	49.59	–0.39	0.96	1.72	1.586×10^3	II	Szymczak et al. (2000)
19303+1651	19303+1651	19 30 20.3	+16 51 04.5	52.66	–1.09	0.64	1.77	1.238×10^2	II	Blaszkiewicz & Kus (2004)
19388+2357	19388+2357	19 38 52.7	+23 57 35.7	59.83	0.67	0.93	2.30	4.334×10^2	II	Slysh et al. (1999)
MMI–145	19410+2336	19 41 04.3	+23 36 42.0	59.78	0.06	0.88	1.83	1.631×10^3	I	Val'tts et al. (2007)
20081+3122	20081+3122	20 08 09.9	+31 22 38.6	69.54	–0.98	1.72	3.11	3.119×10^3	II	Szymczak et al. (2000)
ON1	20081+3122	20 08 09.92	+31 22 41.59	69.54	–0.98	1.72	3.11	3.119×10^3	I	Haschick et al. (1990)
20290+4052	20290+4052	20 29 03.1	+40 52 15.0	79.74	0.99	0.98	2.05	1.367×10^2	II	Blaszkiewicz & Kus (2004)
20350+4126	20350+4126	20 35 04.9	+41 26 02.3	80.87	0.42	1.07	1.95	3.272×10^3	II	Slysh et al. (1999)
21074+4949	21074+4949	21 07 28.47	+49 49 46.09	90.92	1.51	1.02	2.25	7.148×10^2	II	Szymczak et al. (2000)
GL2789	21381+5000	21 38 11.3	+50 00 45.3	94.60	–1.80	0.28	0.51	4.546×10^2	II	Slysh et al. (1999)
R146	21426+6556	21 42 40.1	+65 52 56.9	105.47	9.83	–0.17	0.74	2.119×10^1	I	Kalenskii et al. (1994)
S156A	23030+5958	23 03 05.03	+59 58 09.38	110.11	0.04	0.81	1.59	1.833×10^3	II	Bachiller et al. (1990)
NGC7538S	23116+6111	23 11 36.11	+61 10 33.04	111.53	0.76	0.87	1.46	1.414×10^4	I	Haschick et al. (1989)

G32.74–0.07 and G39.10+0.48 are blended, but the relevant ^{13}CO emission spectra can be distinguished well. So, these four sources are also analyzed. In the 55 sources, we detected significant ^{12}CO and ^{13}CO signals, but only 60% of them showed obvious C^{18}O signals. No differences are found in the detection rate of $J = 1 - 0$ lines of CO isotopes between Class I and Class II methanol maser sources. These 55 sources present profuse ^{13}CO line profiles. About 40% of them have wings and nearly 20 sources have more than one component. We fitted these ^{13}CO lines with a Gaussian function. We distinguish between several different non-Gaussian ^{13}CO line profiles with the following characteristics: (a) wings; (b) red wing; (c) blue wing; (d) red shoulder; (e) red asymmetry; (f) blue asymmetry; (g) flat top; (h) two or three components.

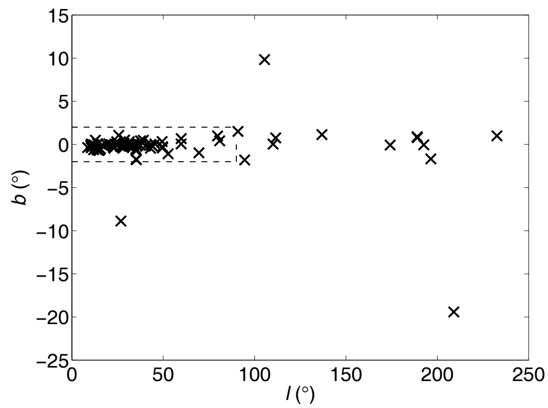

Fig. 1 Galactic distribution of the sources surveyed. The dashed lines indicate the region with $|b| < 2^\circ$ and $0 < l < 90^\circ$. Nearly all the sources are crowded on the Galactic plane, and in the longitude range, 0° to 60°, the plane is very densely populated.

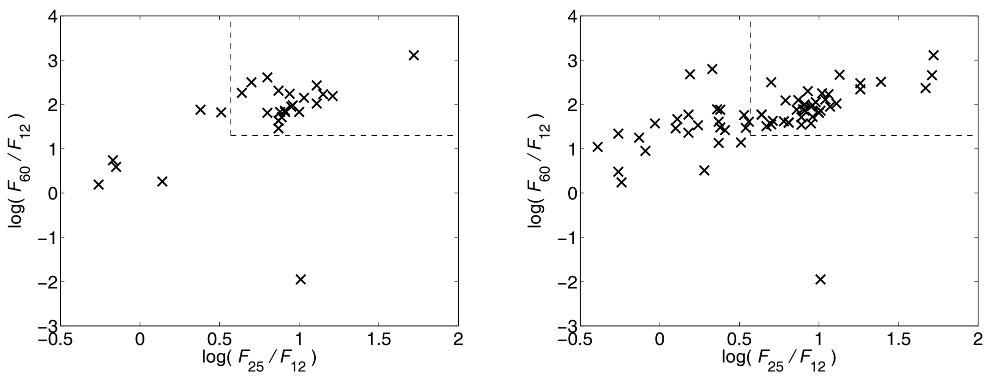

Fig. 2 *Left panel* describes the color-color distribution of the 29 Class I methanol maser sources and the *right panel* is for the 69 Class II methanol maser sources. The color box of UC HII regions established by Wood & Churchwell (1989) is indicated by the dashed lines in both panels.

The identities of these ^{13}CO spectral characteristics are presented in Col. (12) of Table 2. Possible clues of high velocity gas were detected in five sources of Class I and nine sources of Class II methanol maser sources (see the last column of Table 2). There seem to be no differences in the high velocity gas detection rate between Class I and Class II methanol maser sources. Detailed investigations with denser molecular probes such as HCN and CS are needed.

Observation parameters, including the antenna temperature $T_A{}^*$, $V_{\rm LSR}$ and the ^{13}CO line widths (FWHM) of each component, were obtained and are shown in Cols. (2)–(4) of Table 2. Cols. (5)–(6) list the distances from the Galactic center (R) and the Sun (D). Nine components cannot provide available distances from fitting the Galactic rotational curve. Col. (7) presents the bolometric luminosity calculated with the formation in Casoli et al. (1986):

$$L_{(5-1000\,\mu{\rm m})} = 4\pi\, D^2 \times 1.75 \times (F_{12}/0.79 + F_{25}/2 + F_{60}/3.9 + F_{100}/9.9), \qquad (1)$$

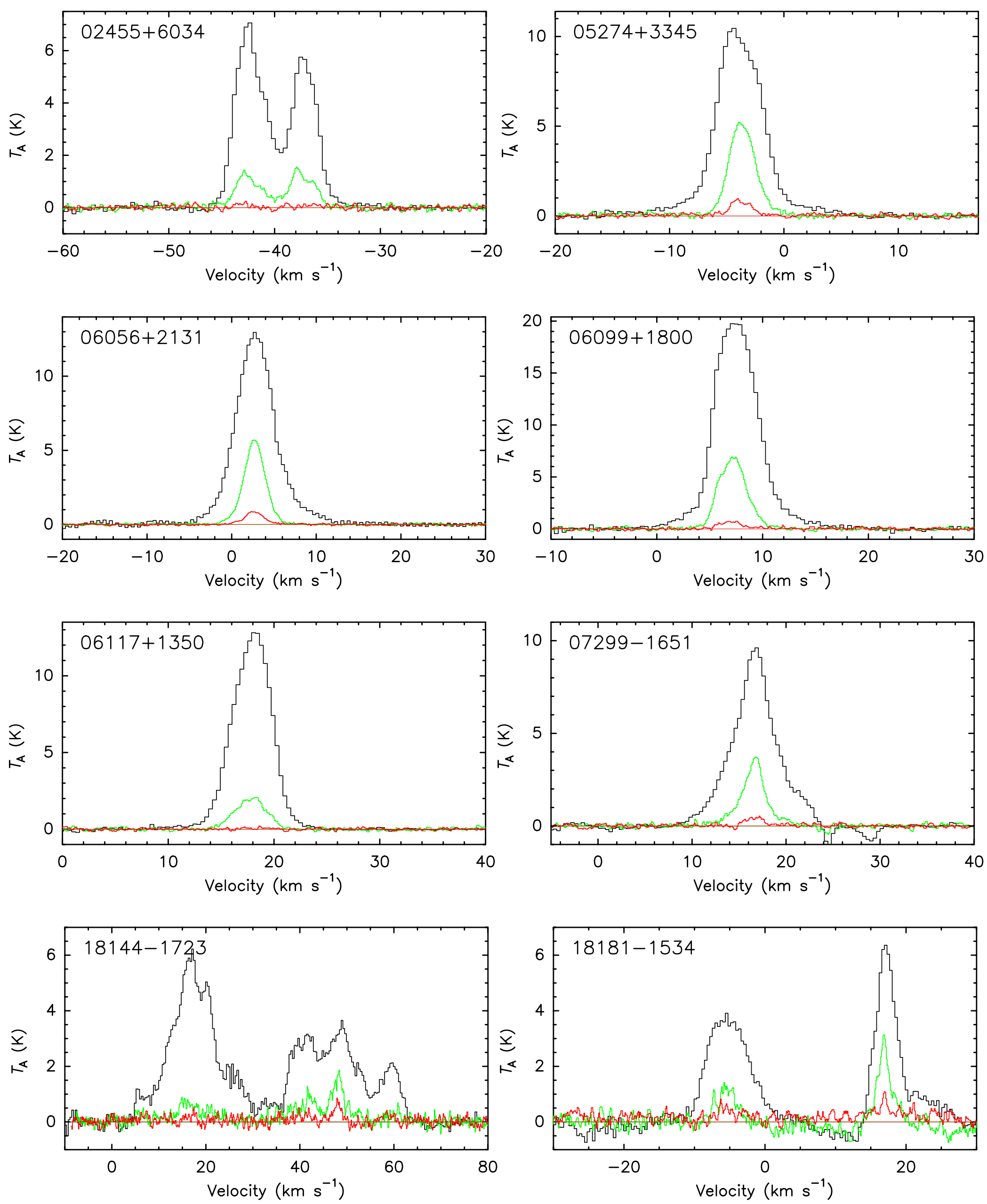

Fig. 3 Spectra of emission line samples. The gray, green and red lines (see electronic version) represent ^{12}CO, ^{13}CO and C^{18}O $J = 1 - 0$, respectively. The source names are drawn on the upper-left corners of each panel. The ^{12}CO spectra of IRAS 18414–1723, IRAS 18353–0628, G32.74–0.07 and G39.10+0.48 are blended, but the respective ^{13}CO emission spectra can be distinguished well. Source G29.86–0.05 is a sample with blended ^{13}CO emission lines. The properties of these ^{13}CO emission line profiles can be found in Col. (12) of Table 2.

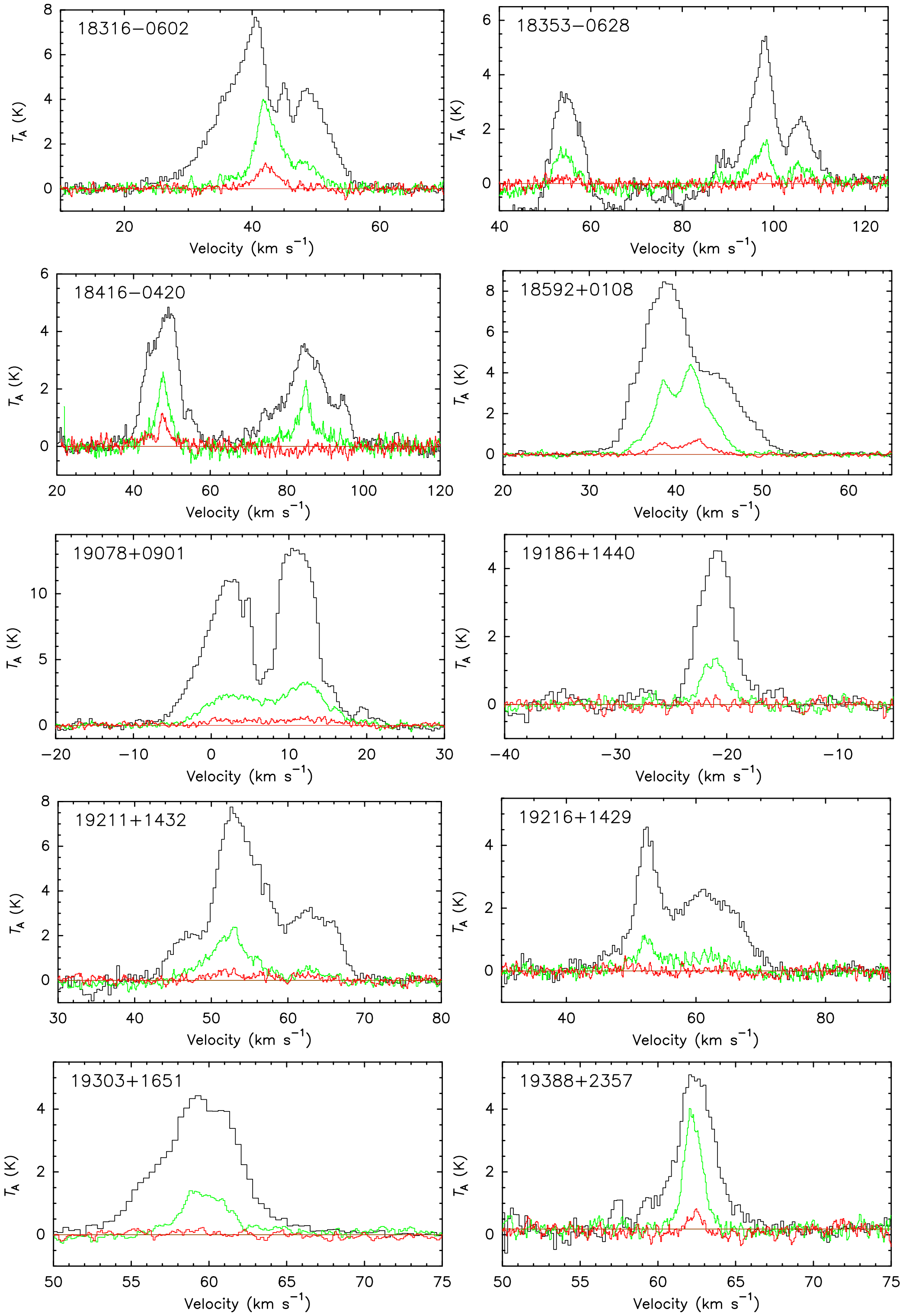

Fig. 3 — *Continued.*

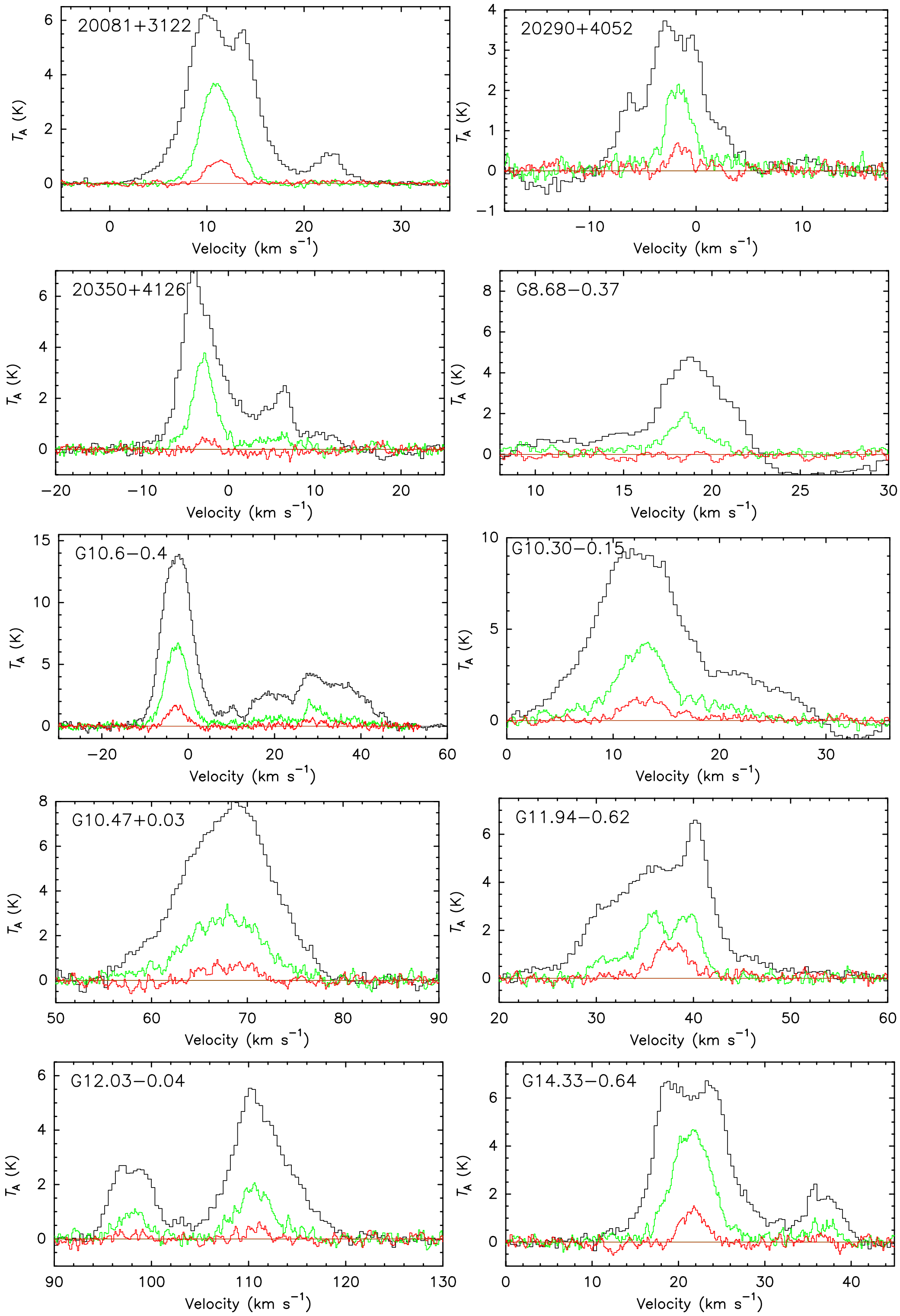

Fig. 3 — *Continued.*

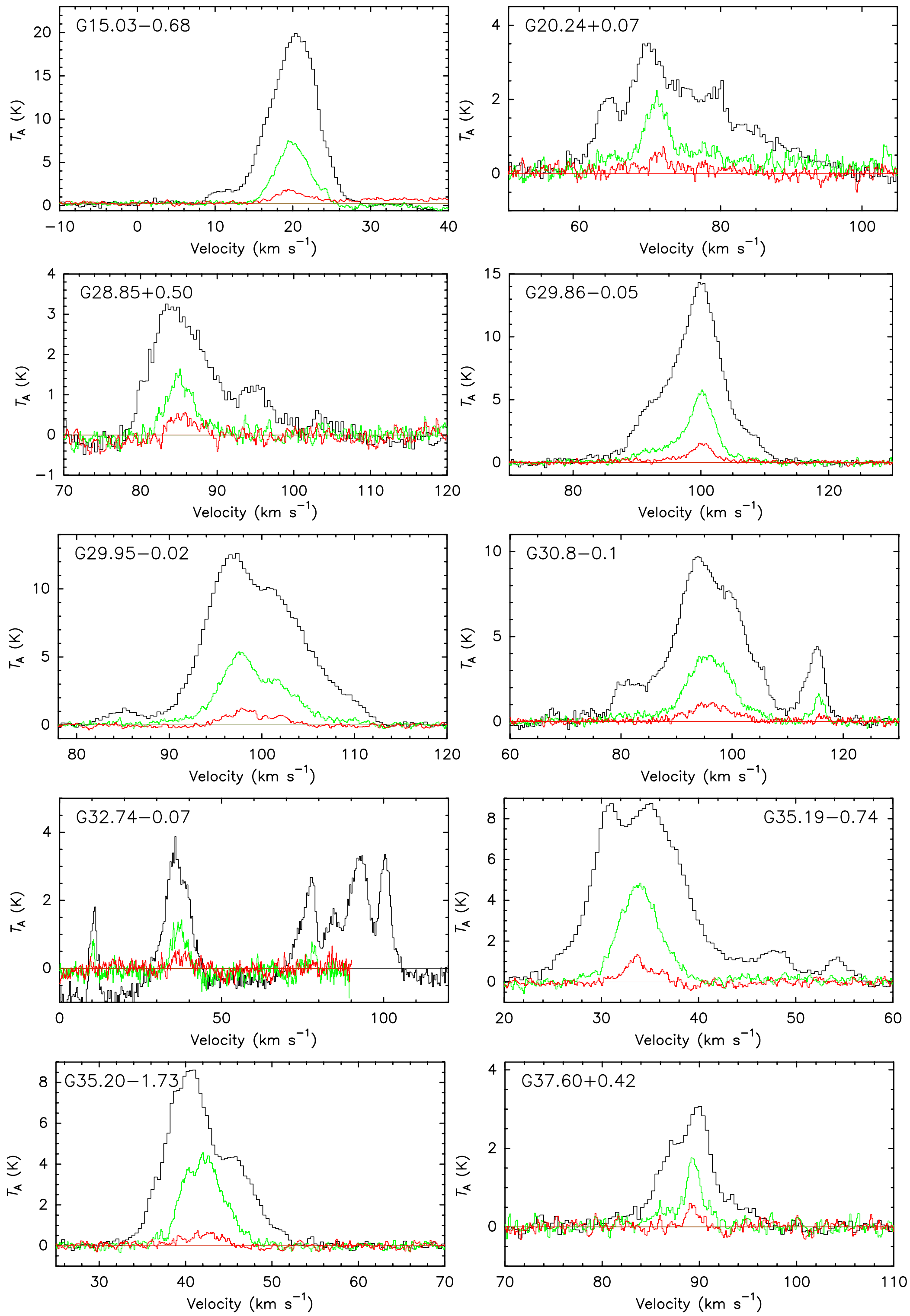

Fig. 3 — *Continued.*

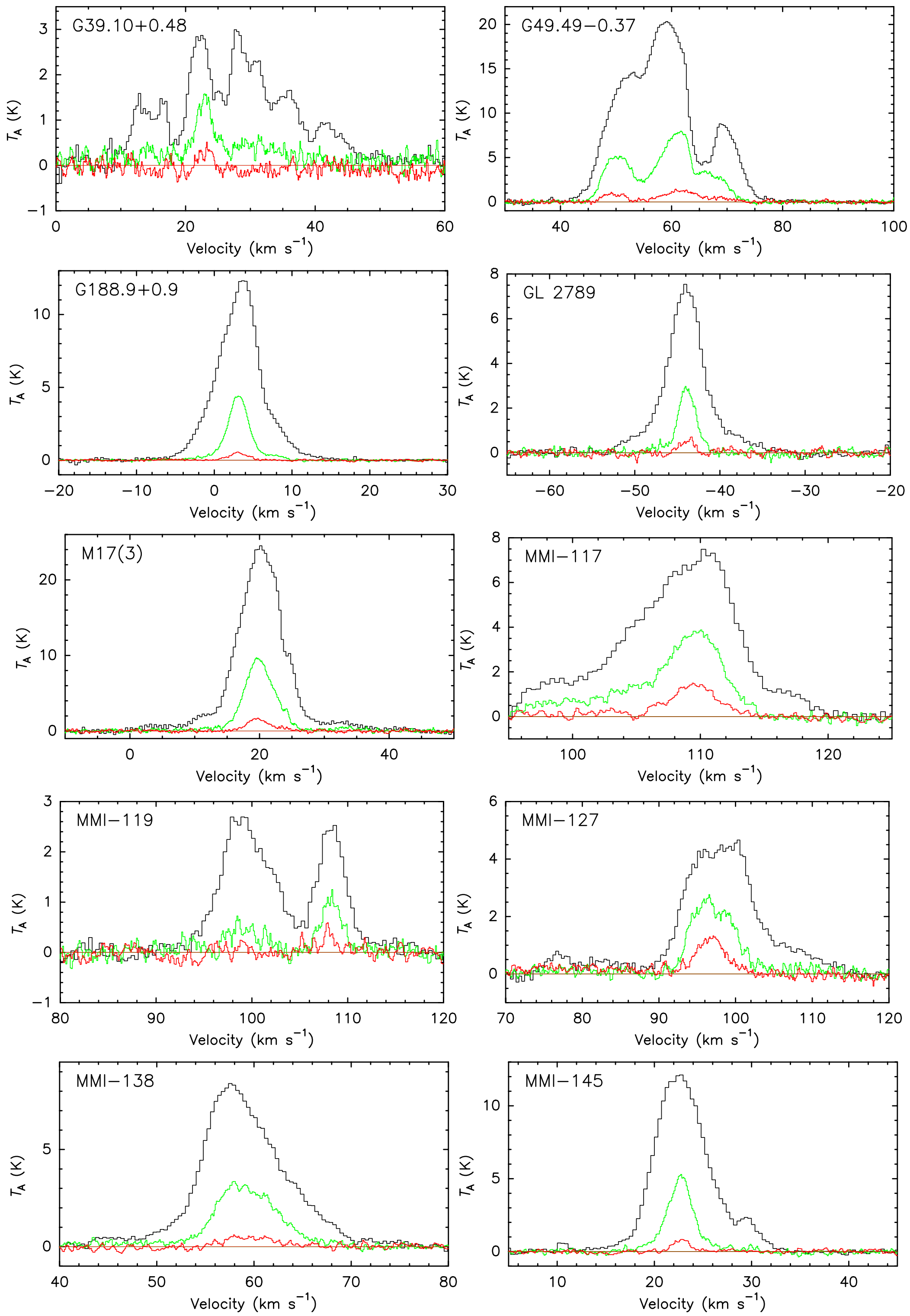

Fig. 3 — *Continued.*

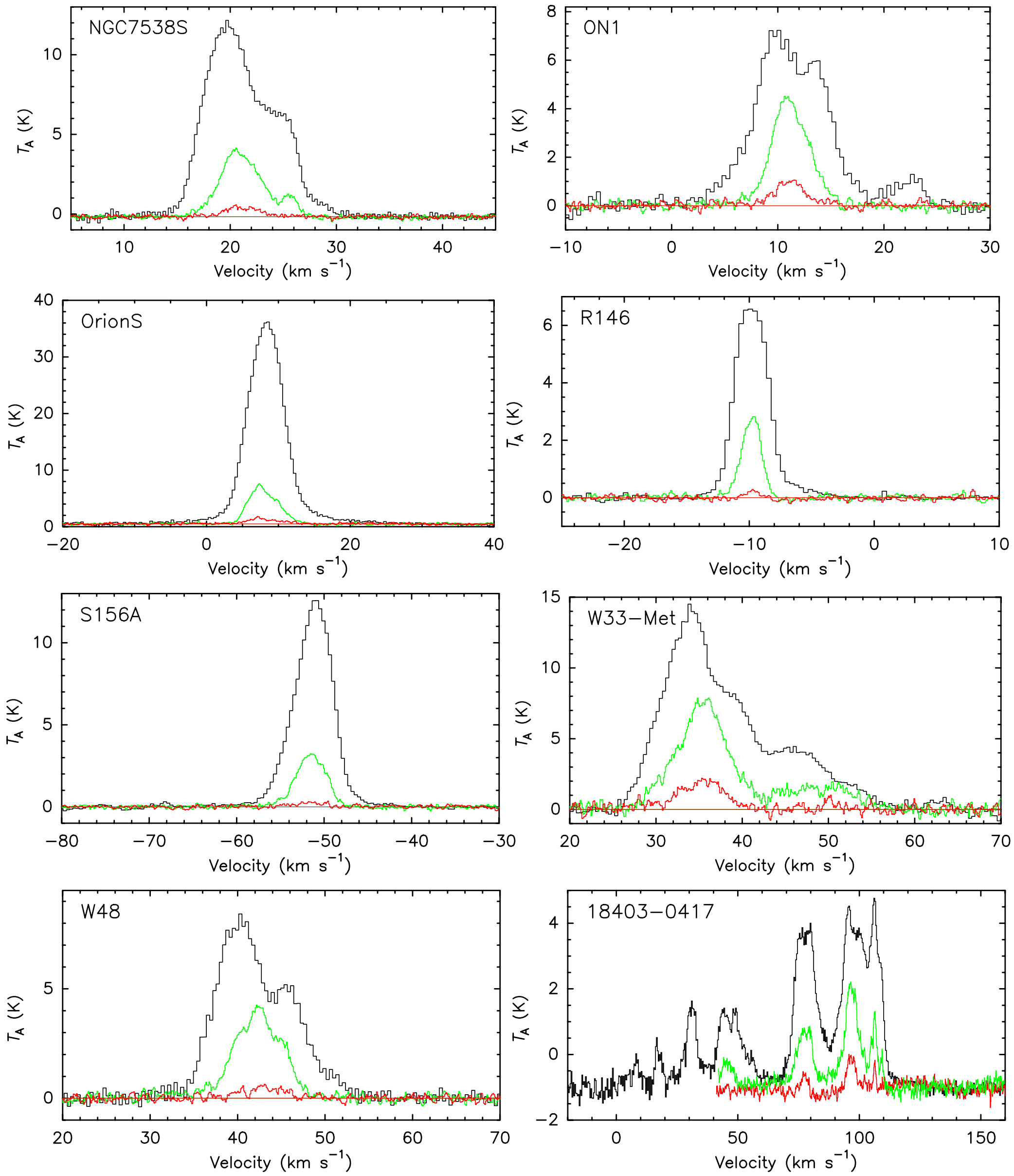

Fig. 3 — *Continued.*

where D is the distance. Fifty of the 55 sources have $L_{\rm bol}>10^3 L_{\odot}$, which are supposed to be massive star formation regions.

Assuming that ^{12}CO is optically thick, we derived the excited temperatures $T_{\rm ex}$ following Garden et al. (1991). Assuming that ^{13}CO is optically thin, then the optical depth and column density of ^{13}CO can be straightforwardly obtained under the local thermodynamic equilibrium assumption (LTE). With the abundance ratio [H_2]/[^{13}CO]=8.9×10^5, the column density of H_2 was calculated. The results are listed in Cols. (8)–(11).

Table 2 Sources with Resolved Components

Name (1)	$T_A{}^*$ (K) (2)	V_{LSR} (km s^{-1}) (3)	FWHM (km s^{-1}) (4)	R (kpc) (5)	D (kpc) (6)	L_{bol} ($L_\odot$) (7)	T_{ex} (K) (8)	τ_{13} (9)	$N(^{13}CO)$ (10^{16} cm^{-2}) (10)	$N(H_2)$ (10^{22} cm^{-2}) (11)	Pro (12)
02455+6034	1.3(9)	–42.51(0)	2.78(1)	12.19	4.52	1.1×10^4	16.04	0.22	0.9	0.8	d
	1.2(8)	–37.40(0)	2.78(3)	11.62	3.86	8.2×10^3	13.22	0.27	0.8	0.7	d
OrionS	6.5(1)	7.80(4)	4.73(7)	9.39	1.06	9.4×10^3	47.92	0.26	14.2	1.2	e
06056+2131	5.8(0)	2.66(9)	2.99(5)	9.38	0.89	4.0×10^3	19.99	0.81	5.3	4.7	
G188.9+0.9	4.4(4)	3.06(8)	3.22(6)	9.52	1.03	3.1×10^3	18.78	0.61	3.8	3.4	a
06117+1350	2.1(5)	17.80(1)	3.42(8)	12.25	3.86	5.8×10^4	20.52	0.22	1.7	1.6	f
07299–1651	3.4(7)	16.50(3)	2.89(3)	9.57	1.62	8.5×10^3	15.04	0.64	2.4	2.1	a
G10.47+0.03	2.8(1)	67.65(2)	9.31(2)	3.08	5.69	3.8×10^5	13.18	0.61	5.8	5.2	g
G10.6–0.4	6.5(3)	–2.65(0)	6.00(7)	9.26	17.48	8.2×10^6	20.99	0.89	12.7	11.4	g
	1.4(3)	29.08(3)	5.05(9)	4.92	3.69	3.7×10^5	7.77	0.69	8.5	7.6	d
G11.94–0.62	2.5(7)	35.78(9)	2.86(1)	4.72	3.94	1.0×10^5	8.71	1.39	2.0	1.8	c,g
	2.6(6)	39.48(0)	3.05(2)	4.5	4.17	1.2×10^5	7.51	4.45	5.4	4.9	g
18144–1723	0.5(0)	16.73(0)	6.23(0)	6.45	2.13	6.7×10^3	9.92	0.13	0.5	0.5	g
	0.6(3)	41.65(7)	6.18(8)	4.68	4.04	2.4×10^4	6.88	0.32	0.7	0.6	
	1.4(6)	48.15(8)	2.99(0)	4.36	4.39	2.8×10^4	7.15	0.89	1.0	0.9	
G14.33–0.64	4.6(3)	21.52(3)	5.44(6)	6.1	2.51	2.2×10^4	12.54	1.61	8.3	7.4	g
G15.03–0.68	8.1(9)	20.00(1)	5.34(6)	6.31	2.29	4.9×10^5	32.03	0.61	17.0	15.2	e,g
18181–1534	1.1(7)	–5.44(3)	3.31(2)	9.54	17.44	2.5×10^5	7.8	0.52	0.7	0.7	g
	2.6(2)	16.90(6)	2.45(5)	6.65	1.94	3.1×10^3	10.13	0.94	1.5	1.4	e
18316–0602	3.4(7)	42.10(5)	4.09(5)	5.9	3.06	3.0×10^4	11.16	1.21	3.8	3.4	e
	1.1(0)	47.59(4)	6.06(9)	5.66	3.36	3.6×10^4	8.01	0.46	1.2	1.1	g
18353–0628	1.3(3)	54.12(6)	5.45(8)	5.41	3.7	3.8×10^4	8.46	0.52	1.4	1.2	g
	1.3(4)	97.32(5)	5.18(4)	4.15	5.75	9.2×10^4	9.31	0.44	1.3	1.1	f
	0.6(4)	105.88(4)	4.03(7)	3.97	6.19	1.1×10^5	6.09	0.43	0.5	0.4	g
MMI–119	0.4(5)	99.18(8)	4.04(0)	4.18	5.87	2.7×10^4	6.35	0.26	0.3	0.3	g
	1.0(2)	108.28(2)	2.51(4)	3.99	6.41	3.2×10^4	6.18	0.77	0.6	0.5	g
G29.95–0.02	4.6(0)	98.68(2)	8.53(9)	4.43	6.1	9.0×10^5	17.75	0.71	10.6	9.5	d
MMI–127	2.4(9)	96.94(9)	6.25(6)	4.56	6.17	1.3×10^5	8.53	1.39	4.3	3.8	e
G32.74–0.07	0.8(7)	10.29(3)	0.97(5)	7.92	0.7	0.5×10^3	6.15	0.62	0.2	0.2	
	1.2(9)	36.96(6)	5.27(2)	6.51	2.54	6.9×10^3	7.59	0.64	1.4	1.2	g
	0.7(0)	78.24(1)	2.51(4)	5.1	4.94	2.6×10^4	5.56	0.61	0.4	0.3	g
G37.60+0.42	1.5(0)	89.37(2)	2.27(0)	5.07			6.55	1.23	0.9	0.8	c
18592+0108	2.3(4)	39.35(4)	2.54(0)	6.51	2.66	1.9×10^5	13.53	0.46	1.2	1.1	
	3.8(6)	42.89(3)	4.44(0)	6.37	2.87	2.2×10^5	13.53	0.92	4.4	3.9	
19078+0901	3.0(1)	12.04(5)	6.78(8)	7.97	0.76	2.0×10^4	21.05	0.32	5.1	4.6	e
	2.3(1)	2.78(8)	7.96(5)	8.47	12.35	5.5×10^6	16.96	0.32	4.0	3.6	g
MMI–138	3.1(0)	59.12(4)	7.02(8)	6.19	4.71	3.3×10^5	13.13	0.7	5.0	4.5	f
19186+1440	1.2(7)	–21.10(7)	2.68(5)	9.93	13.08	4.9×10^4	8.89	0.45	0.6	0.6	g
19216+1429	0.8(5)	52.39(3)	4.38(8)	6.5	4.88	9.8×10^4	7.79	0.35	0.7	0.6	g
	0.4(8)	61.16(1)	8.16(4)	6.24			6.32	0.28	0.7	0.6	
19303+1651	1.2(8)	59.73(6)	3.96(1)	6.36			8.76	0.46	14.3	12.7	b,i
19388+2357	3.0(3)	34.50(6)	2.74(5)	7.26			8.23	3.34	4.3	3.8	
MMI–145	4.9(2)	22.67(2)	3.22(4)	7.68	2.05	1.2×10^4	18.37	0.74	4.4	4.0	a
20081+3122	4.2(8)	11.09(7)	4.02(3)	8.17	1.13	5.2×10^3	11.77	1.64	5.6	5.0	
20290+4052	2.0(1)	–1.62(4)	2.93(8)	8.7	3.91	3.0×10^3	9.12	0.99	1.6	1.4	g
20350+4126	3.5(0)	-2.87(0)	3.13(0)	8.75	3.83	6.5×10^4	13.69	0.96	3.3	3.0	c
GL2789	2.8(7)	–43.86(8)	2.52(5)	10.89	6.16	8.6×10^4	15	0.6	1.9	1.7	c
R146	3.0(0)	–9.73(9)	1.62(9)	9.07			15.38	0.61	1.3	1.2	
S156A	3.0(6)	–51.51(2)	4.16(0)	11.63	5.54	1.3×10^5	27.38	0.26	4.3	3.8	f
05274+3345	5.1(9)	–3.66(5)	2.63(6)	10.41	1.92	5.3×10^3	16.42	1	4.0	3.6	
06099+1800	6.9(1)	7.15(2)	3.07(6)	10.21	1.74	2.9×10^4	29.03	0.56	7.5	6.7	
G8.68–0.37	1.4(2)	18.53(9)	2.04(6)	5.44	3.12	6.3×10^4	9.79	0.43	0.5	0.5	
	3.8(3)	36.65(8)	7.04(4)	3.98	4.64	1.4×10^5	13.81	0.87	6.7	6.1	e
G10.30–0.15	3.7(1)	12.86(8)	5.90(6)	6.43	2.12	8.9×10^4	14.94	0.71	5.4	4.8	b

Table 2 — *Continued.*

Name (1)	$T_A{}^*$ (K) (2)	V_{LSR} (km s^{-1}) (3)	FWHM (km s^{-1}) (4)	R (kpc) (5)	D (kpc) (6)	L_{bol} $(L_\odot)$ (7)	T_{ex} (K) (8)	τ_{13} (9)	$N(^{13}CO)$ (10^{16} cm^{-2}) (10)	$N(H_2)$ (10^{22} cm^{-2}) (11)	Pro (12)
G12.03–0.04	0.9(3)	98.05(1)	3.43(3)	2.62	6.38	5.0×10^4	6.77	0.53	0.6	0.6	g
	1.7(3)	110.61(5)	3.96(9)	2.41	6.69	5.4×10^4	9.48	0.58	1.4	1.2	g
W33-Met	6.9(7)	35.43(3)	6.44(0)	4.89	3.78	5.0×10^4	19.27	1.2	15.7	14.0	g
	1.1(2)	48.56(1)	7.62(6)	4.2	4.53	7.2×10^4	8.61	0.41	1.5	1.4	
M17(3)	9.1(3)	19.98(6)	5.41(0)	4.12	4.42	1.8×10^6	32.58	0.69	20.1	18.0	e
G20.24+0.07	1.6(2)	71.06(4)	4.39(8)	4.35	4.77	9.7×10^3	6.65	1.35	2.0	1.8	a
MMI–117	3.4(9)	109.22(3)	6.20(4)	3.83	6.32	1.2×10^5	11.64	1.1	5.7	5.0	c
G28.85+0.50	1.4(0)	85.13(2)	4.42(6)	4.68	5.2	8.2×10^3	6.9	0.92	1.4	1.3	e
18416–0420	2.1(2)	47.61(3)	4.31(8)	5.83	3.26	1.1×10^5	8.28	1.11	2.2	2.0	c
	1.5(7)	84.78(5)	3.94(3)	4.65	5.17	2.8×10^5	6.3	1.59	1.9	1.7	a
G29.86–0.05	4.9(7)	99.89(3)	5.98(3)	2.24	6.67	1.1×10^6	18.77	0.72	8.3	7.5	c
G30.8–0.1	3.6(8)	95.93(4)	9.04(0)	4.55	5.99	1.8×10^5	14.82	0.71	8.2	7.3	g,a
	1.3(9)	115.63(0)	1.95(7)	4.14			8.46	0.55	0.5	0.5	c
G35.19–0.74	4.5(9)	33.88(3)	4.92(2)	6.75	2.31	2.2×10^4	13.24	1.34	6.8	6.1	g
G39.10+0.48	1.2(4)	22.96(1)	3.10(0)	7.36	1.55	0.6×10^3	6.65	0.84	0.9	0.8	e,g
G35.20–1.73	4.2(6)	41.99(4)	5.59(8)	6.41	2.82	2.1×10^5	13.83	1.04	6.5	5.8	f
W48	3.8(6)	42.37(7)	6.21(5)	6.39	2.84	2.2×10^5	13.34	0.95	6.2	5.6	d,f
19211+1432	2.0(4)	52.32(3)	7.51(4)	6.5	4.85	6.4×10^3	11.96	0.47	3.1	2.8	c,e
	0.5(5)	63.10(1)	4.83(4)	6.19			7.01	0.26	0.5	0.4	
G49.49–0.37	5.2(5)	50.31(9)	6.08(8)	6.56	4.37	5.9×10^5	15.62	1.14	9.7	8.6	g
	7.6(0)	60.61(9)	6.90(8)	6.26			28.42	0.66	19.0	17.0	g
	2.5(3)	68.13(2)	5.20(8)	6.05			13.14	0.53	2.8	2.5	g
ON1	4.3(3)	11.13(4)	4.11(5)	8.17	1.14	5.3×10^3	11.9	1.63	5.8	5.2	e
NGC7538S	5.0(0)	-56.14(8)	6.57(9)	12.05	5.98	9.1×10^5	27.4	0.48	12.2	11.0	f
	1.4(7)	-48.95(9)	2.72(0)	11.47	5.19	6.9×10^5	15.19	0.26	0.9	0.8	g

a: wings, b: red wing, c: blue wing, d: red shoulder; e: red asymmetry, f: blue asymmetry, g: flat top, h: two or three components.

Figure 4 presents a plot of bolometric luminosity $L_{\rm bol}$ vs. ^{13}CO line widths for the 55 sources. The linear fit gives: $\log(L_{\rm bol}/L_\odot) = 2.5\log({\rm FWHM/km\ s^{-1}}) + 3.2$; the correlation coefficient $r = 0.52$. From Col.(4) of Table 2, we can see that almost all the ^{13}CO lines, except for one component from the source G32.74–0.07, have line widths larger than 1.3 km s^{-1}, which is the typical line width for low-mass sources according to Myers et al. (1983). Also, 57 out of these 79 resolved components have ^{13}CO line widths larger than 3 km s^{-1}, indicating possible high-mass star formation regions (Wu et al. 2003). The average line width of ^{13}CO is 4.5 km s^{-1}, similar to that detected by Purcell et al. (2009). These results indicate that sources with large line widths tend to form high-mass stars. This trend is consistent with the results of Wang et al. (2009). We also fitted the C^{18}O lines of 30 sources and found they have line widths of 4 km s^{-1} on average, smaller than the ^{13}CO lines. The ^{13}CO line antenna temperatures of about one half of these 30 sources are 5.5 times larger than those of the C^{18}O lines, and about 75% of the integrated intensities of the ^{13}CO lines are 5 times larger than those of the C^{18}O lines. However, the center velocities of the C^{18}O lines match the ^{13}CO lines very well, suggesting that the ^{13}CO emissions and the C^{18}O emissions may be from the same region in the cloud.

3.3 Mapping Results and Discussion

Two sources, IRAS 06117+1350 and IRAS 07299–1651, were mapped. Figure 5 presents the contours of the integrated intensities of ^{13}CO lines. IRAS 06117+1350 has two cores and we label them as 06117+1350-SE and 06117+1350-NW. One core was detected in IRAS 07299–1651. The posi-

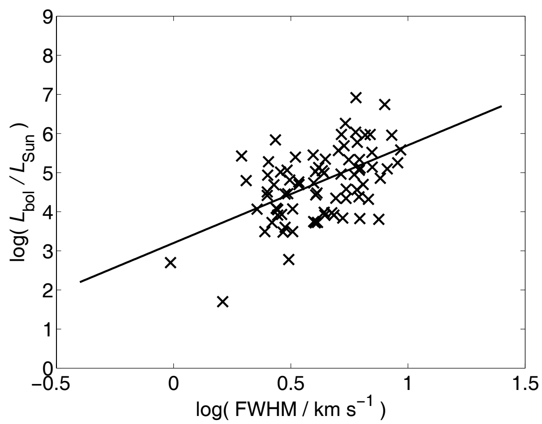

Fig. 4 Bolometric luminosity ($L_{\rm bol}$) versus ^{13}CO line width. The linear fit of $L_{\rm bol}$ and FWHM is: $\log(L_{\rm bol}/L_{\odot}) = 2.5\log({\rm FWHM/km\ s^{-1}}) + 3.2$; the correlation coefficient $r = 0.52$.

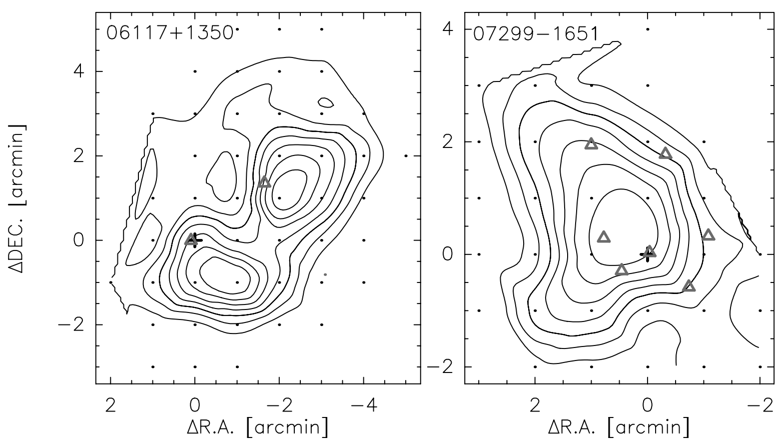

Fig. 5 Contours of the integrated intensities of ^{13}CO lines. *Left*: IRAS 06117+1350, *Right*: IRAS 07299–1651. The positions of IRAS sources are marked with "+" and the MSX sources are shown as triangles.

tions of the IRAS sources are marked with "+" and the Midcourse Space Experiment (MSX) sources are shown as triangles.

We calculated the masses of the cores under the LTE assumption. We also calculated the virial mass using the equation from Ungerechts et al. (2000). The physical results of these cores are listed in Table 3. The two cores in IRAS 06117+1350 have a virial mass smaller than the core mass, indicating they are stable and the gas motions are gravitationally bound. Specifically, all of our cores are far away from UC HII regions. No Spitzer/IRAS data are available for the mapped sources. The core in IRAS 07299–1651 has one IRAS source and three MSX sources. The northwest core of IRAS 06117+1350 is far away from any IRAS source but is associated with one MSX source about

Table 3 Physical Parameters of the ^{13}CO Molecular Cores

Name	α(B1950) (h m s)	δ(B1950) (° ′ ″)	$V_{\rm LSR}$ (km s^{-1})	FWHM (km s^{-1})	D (kpc)	$T_{\rm ex}$ (K)	R (pc)	$N(H_2)$ (10^{22} cm^{-2})	$M_{\rm core}$ ($M_\odot$)	$M_{\rm vir}$ ($M_\odot$)
06117+1350–SE	06 11 46.4	+13 50 32.7	16.48(2)	3.34(9)	3.86	18.47	1.45	2.1	4.0×10^3	3.4×10^3
06117+1350–NW	06 11 46.4	+13 50 32.7	16.68(3)	2.95(7)	3.86	17.29	1.42	2.0	3.6×10^3	2.6×10^3
07299–1651	07 29 55.0	–16 51 47.2	16.50(3)	2.89(3)	1.62	15.04	0.79	2.2	1.2×10^3	1.4×10^3

$0.5'$ from the ^{13}CO emission peak. Since no 6 cm emissions are associated with these two cores, they can be identified as HMPOs or UC HII precursors (e.g. Wu et al. 2006 and references therein). The southeast core of IRAS 06117+1350 is separated from any IRAS source and MSX source, indicating an evolutionary stage earlier than pre-UC HII.

4 SUMMARY

A survey of CO and its isotopes at the locations traced by methanol masers was performed. Fifty-five sources are further studied. They all have $J = 1 - 0$ emissions of ^{12}CO and ^{13}CO, but only 60% of them have significant C^{18}O emissions. No differences in either the CO detection rate or the high velocity gas detection rate were found between Class I and Class II methanol maser sources. Fifty of these 55 sources are associated with luminous IRAS sources ($L_{\rm bol} > 10^3 L_\odot$). The relationship between the bolometric luminosity of the associated IRAS sources and ^{13}CO line widths can be described well as: $\log(L_{\rm bol}/L_\odot) = 2.5 \log({\rm FWHM/km\ s^{-1}}) + 3.2$. About three quarters of the resolved components have ^{13}CO line widths much larger than 3 km s^{-1}. These results show that molecular cores with large line widths tend to form high-mass stellar objects. In 30 sources, ^{13}CO lines have larger line widths and antenna temperatures than C^{18}O lines. However, the center velocities of C^{18}O lines match those of ^{13}CO lines very well, suggesting that ^{13}CO emissions and C^{18}O emissions may be from the same region in the cloud.

Two cores are detected in IRAS 06117+1350 and one core in IRAS 07299–1651. The two cores in IRAS 06117+1350 have a virial mass less than the core mass, but the core in IRAS 07299–1651 has a virial mass larger than the core mass. The core in IRAS 07299–1651 and the northwest core of the source IRAS 06117+1350 may be pre-UC HII or HMPOs and the southeast core of IRAS 06117+1350 seems to be at an earlier evolutionary stage than the pre-UC HII phase.

Acknowledgements We are grateful to all the staff of Qinghai station of PMO for their assistance during the observations. N. C. Sun and Y. A. Mao also deserve our thanks for their help and discussions. This project is supported by the National Natural Science Foundation of China (Grant Nos. 10733030 and 10873019).

References

Bachiller, R., Menten, K. M., Gómez-González, J., & Barcia, A. 1990, A&A, 240, 116
Blaszkiewicz, L., & Kus, A. J. 2004, A&A, 413, 233
Casoli, F., Dupraz, C., Gerin, M., Combes, F., & Boulanger, F. 1986, A&A, 169, 281
Caswell, J. L., Gardner, F. F., Norris, R. P., et al. 1993, MNRAS, 260, 425
Garden, R. P., Hayashi, M., Gatley, I., Hasegawa, T., & Kaifu, N. 1991, ApJ, 374, 540
Guilloteau, S., & Lucas, R. 2000, in ASP Conf. Ser. 217, Imaging at Radio through Submillimeter Wavelengths, eds. J. G. Mangum, & S. Radford, 299
Haschick, A. D., & Baan, W. A. 1989, ApJ, 339, 949
Haschick, A. D., Menten, K. M., & Baan, W. A. 1990, ApJ, 354, 556
Kalenskii, S.V., Liljeström, T., Val'tts, I. E., Vasil'kov, V. I., Slysh, V. I., & Urpo, S. 1994, A&AS, 103, 129

Minier, V., Ellingsen, S. P., Norris, R. P., & Booth, R. S. 2003, A&A, 403, 1095
Myers, P. C., Linke, R. A., & Benson, P. J. 1983, ApJ, 264, 517
Plume, R., Jaffe, D. T., & Evans, N. J. II. 1992, ApJS, 78, 505
Purcell, C. R., Longmore, S. N., Burton, M. G., et al. 2009, MNRAS, 394, 323
Shu, F. H., Adams, F. C., & Lizano, S. 1987, ARA&A, 25, 23
Slysh, V. I., Kalenskii, S. V., Val'tts, I. E., & Otrupcek, R. 1994, MNRAS, 268, 464
Slysh, V. I., Val'tts, I. E., Kalenskii, S. V., et al. 1999, A&AS, 134, 115
Sobolev, A. M., et al. 2006, arxiv:astro-ph/0601260
Szymczak, M., Hrynek, G., & Kus, A. J. 2000, A&AS, 143, 269
Szymczak, M., Kus, A. J., Hrynek, G., Kepa, A., & Pazderski, E. 2002, A&A, 392, 277
Ungerechts, H., Umbanhowar, P., & Thaddeus, P. 2000, ApJ, 537, 221
Val'tts, I. E., & Condon, G. M. 2007, Astronomy reports, 51, 519
Wang, K., Wu, Y., Ran, L., Yu, W., & Miller, M. 2009, A&A, 507, 369
Wood, D. O. S., & Churchwell, E. 1989, ApJ, 340, 265
Wu, Y., Wu, J., & Wang, J. 2003, Chinese Physics Letters, 20, 1409
Wu, Y., Wei, Y., Zhao, M., Shi, Y., Yu, W., Qin, S., & Huang, M. 2004, A&A, 426, 503
Wu, Y., Zhang, Q., Yu, W., Miller, M., Mao, R., Sun, K., & Wang, Y. 2006, A&A, 450, 607